INSTITUTE OF PHYSICS PUBLISHING and INTERNATIONAL ATOMIC ENERGY AGENCY NUCLEAR FUSION

Nucl. Fusion **44** (2004) S55–S63 PII: S0029-5515(04)76842-8

Modelling of the field line penetration and force transfer by the dynamic ergodic divertor of TEXTOR

K.H. Finken[1], **S.S. Abdullaev**[1], **M. Jakubowski**[1], **M. Lehnen**[1] **and G. Sewell**[2]

[1] Institut für Plasmaphysik, Forschungszentrum Jülich GmbH, EURATOM Association, D-52425 Jülich, Germany[a]

[2] Mathematics Department, University of Texas at El Paso, El Paso, USA

E-mail: k.h.finken@fz-juelich.de

Received 12 November 2003, accepted for publication 24 February 2004
Published 28 May 2004
Online at stacks.iop.org/NF/44/S55
doi:10.1088/0029-5515/44/6/S06

Abstract

For describing the penetration of the external dynamic ergodic divertor magnetic field into the plasma, a single fluid magnetohydrodynamic model has been applied which contains all three components of the magnetic and electric field, the electrical currents and the flow pattern. The set of equations is solved numerically. The analysis shows that the external magnetic field penetrates nearly unperturbed into the plasma edge; at the resonance layer, where the external coils are parallel to the internal magnetic field lines, a strong shielding current is generated. Depending on the frequency difference between the external field and the plasma, the width and the amplitude of the shielding current varies: With increasing frequency, the amplitude and the width of the resonant layer grows while with decreasing frequency both quantities are diminished. The model predicts that the shielding current is connected with a localized flow of the plasma. The force transfer function is calculated from the integration of the $j \times B$ term. Differences between the expected edge and core interactions are discussed.

PACS numbers: 52.35.Bj, 52.35.Vd

1. Introduction

At the TEXTOR tokamak, a new experimental device has been installed recently, the dynamic ergodic divertor, DED [1]. This device is an extremely versatile tool. It allows the generation of either a predominantly ergodic layer at the plasma edge, or of a mainly laminar zone or of a rotating field pattern. The ergodic and laminar zones differ in the connection length of the magnetic field lines intersecting the wall. In the ergodic zone, the connection length is longer than the Kolmogorov length while they are shorter in the laminar zone. The Kolmogorov length L_K is a characteristic length for ergodic structures and it denotes the distance in which initially adjacent orbits (here magnetic field lines) separate; L_K is proportional to the amplitude of the perturbing field $b_{rm,n}$ to the power of $L_K \sim b_{rm,n}^{2/3}$. A detailed analysis of the structures generated by the DED field is given by Abdullaev *et al* [2].

A main goal of applying the static or low rotating edge ergodization is to distribute the heat flux over a large wall area. The DED will create an ergodic boundary layer of the plasma and, thus, an improved screening of impurities is expected, for an optimized use of noble gas impurities under high performance RI-mode operation, and for an enhanced particle removal by the pump limiter ALT-II. The expression 'dynamic' refers to a rotating perturbation magnetic field imposed by the DED coils. For the rotation, different frequencies are foreseen such as a few Hertz for distribution of the heating pattern of the divertor strike zones over the large area of the divertor target plate, or frequencies up to 10 kHz which can lead to an unlocking of modes, or impose a differential rotation in the plasma edge and core and improve confinement.

In this context, the high frequency operation of the DED at frequencies between 1 and 10 kHz is of particular interest. The four-phase ac current in the DED coils generates a rotating magnetic field pattern; it is expected that the induced currents impose a torque at the plasma edge. A sheared plasma rotation is considered favourable for tokamak plasmas. The rotation prevents a strong interaction with induced electric currents in the walls which tend to stop the plasma and easily lead to a locked mode and a subsequent disruption. The sheared

[a] Partner in the Trilateral Euregio Cluster.

flow may destroy convective or turbulent cells and thus reduce the otherwise observed anomalous transport of particles and energy towards the wall. The problem of plasma flow relative to a surface of magnetic islands has been the subject of several studies [3–7]. One motivation for studying this problem is the possibility of using deliberately imposed surfaces of moving islands as a means of velocity profile control [8]. Velocity profile control may allow for confinement improvement, since turbulent transport may be impeded by shear of the plasma rotation [9]. The subject studied may also be relevant to the phenomenon of 'locked modes' associated with field errors [10–12]. In addition, plasma rotation may mitigate the ideal and resistive magnetohydrodynamic (MHD) modes.

In the following—after a description of the DED system—the static ergodization pattern is shown first. This section is followed by the formulation of the equations of a new model in which the interaction between the external field and the plasma is described. The model contains the linearized cold fluid MHD equations; however, it includes all three components of the perturbation magnetic field, of the electric field, and of the flow pattern. The set of coupled differential equations is solved by the program package PDE2D. Finally, the results are discussed and conclusions are given.

2. The experimental set-up

The main component of the DED is a set of magnetic perturbation coils the purpose of which is to ergodize the magnetic field structure in the plasma edge region; these coils are located inside the vacuum vessel at the high field side of the torus as shown in figure 1. The set consists of 16 individual coils (four quadruples) plus two compensation coils. The individual perturbation coils, each winding once around the torus, follow the direction of the equilibrium magnetic field of the plasma edge (i.e. helically); the radial location of enhanced interaction where the helical pitch of the coils exactly matches that of the equilibrium field can be fine-tuned, e.g. by varying the plasma current. By this means, a resonant effect of the external perturbation field is obtained on the edge plasma at a pre-selected radius whereby a perturbation current of only 15 kA is sufficient to create a stochastic structure.

The five main perturbation modes (i.e. poloidal and toroidal Fourier mode combinations) are centred at $m/n = 12/4$; this has been selected because it creates only small local perturbations (magnetic islands) and avoids undesired disturbances in the plasma core. By connecting certain perturbation coils in series, the use of lower m and n is possible, which is of interest for exciting and systematically analysing modes located deeper inside the torus. In addition, the power supplies are laid out to allow for a superposition of the base $12/4$ mode with either the $6/2$ mode or the $3/1$ mode. This option allows to some degree a decoupling of the perturbation strength at the plasma edge from its penetration depth into the plasma.

The DED has the unique feature that the perturbation field is not static as in most other devices but that it has the option of rotation. To our knowledge, only the small research tokamak CSTN [13] at Nagoya University has similar features and—at low perturbation current levels—also the TEXT [14] tokamak. The DED can be operated dc, around 50 Hz or at seven frequencies in the band from 1 to 10 kHz. At low perturbation current (1.5 kA), the perturbation field can be applied across the whole frequency band of interest for feedback stabilization experiments.

3. The model

Basic considerations of the penetration of a rotating DED-type perturbation field have been performed by Faulconer and Koch from a wave propagation point of view [15]. It has been shown that the external rotating magnetic field transforms at the edge of the plasma into a compressional Alfvén wave which propagates radially until the external current is parallel to the local magnetic field lines, $kB_0 = 0$, where k is the wave vector and B_0 is the equilibrium magnetic field. At this resonance radius, the compressional wave is transformed

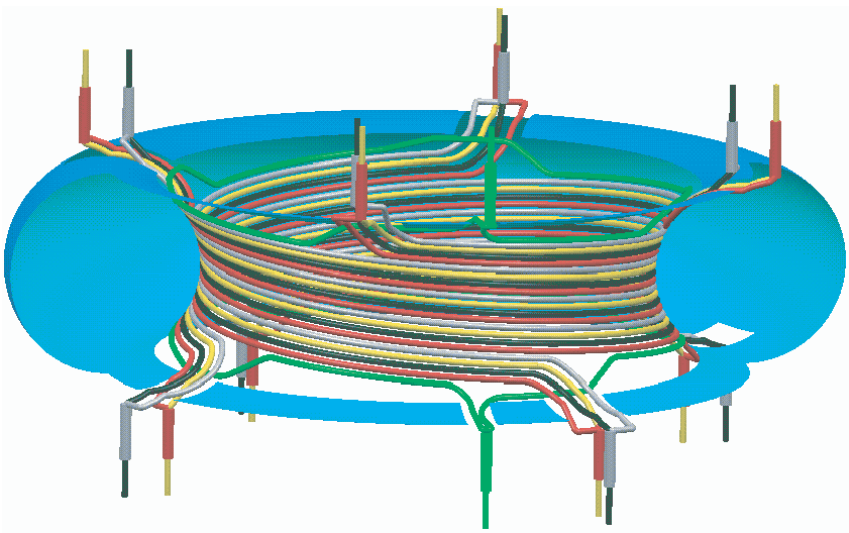

Figure 1. Schematic design sketch of the DED coils. The DED set-up consists of 16 coils; the four different colours indicate the four phases of the electrical currents (0°, 90°, 180°, 270°) which are supplied to the DED coils. For the correct vertical plasma positioning, two compensation coils (green) are added.

into a shear Alfvén wave, which propagates in the resonant layer. Beyond the resonance, the compressional wave can exist again and propagates further inwards. The wave field generates a ponderomotive force, which exerts forces in the axial and poloidal directions as was discussed, e.g. by Elfimov *et al* [16].

Based on this idea, several approaches for the description of the DED-field in the plasma have been performed using a cylindrical approximation of the plasma. In the first attempt, the plasma velocity was treated in a rather simplified way; namely, only the radial velocity component [17, 18] was considered; later the model was extended using additionally the azimuthal one [19]. In this model, we take all components of the linearized perturbed cold MHD equations namely:

$$\mathrm{div}(\boldsymbol{j}) = \mathrm{div}(\boldsymbol{b}) = \mathrm{div}(\boldsymbol{v}) = \mathrm{div}(\boldsymbol{E}) = 0 \tag{1}$$

$$\mathrm{curl}(\boldsymbol{b}(r,\varphi,z,t)) = \mu_0 \boldsymbol{j}(r,\varphi,z,t) \tag{2}$$

$$\mathrm{curl}(\boldsymbol{E}(r,\varphi,z,t)) = -\frac{\partial \boldsymbol{b}(r,\varphi,z,t)}{\partial t} = \mathrm{i}\omega \boldsymbol{b}(r,\varphi,z) \tag{3}$$

$$\boldsymbol{j}(r,\varphi,z,t) = \sigma(\boldsymbol{E} + \boldsymbol{v} \times \boldsymbol{B}_0) \tag{4}$$

$$-\mathrm{i}\omega\rho\boldsymbol{v} = -\mathrm{grad}(p) + \boldsymbol{j} \times \boldsymbol{B}_0 + \boldsymbol{J}_0 \times \boldsymbol{b} \tag{5}$$

The characters $\boldsymbol{j}$, $\boldsymbol{b}$, $\boldsymbol{v}$ and $\boldsymbol{E}$ refer to perturbed quantities that are assumed to be of first-order, while $\boldsymbol{B}_0$ and $\boldsymbol{J}_0$ refer to zero-order equilibrium values of the magnetic field and the current; $\boldsymbol{B}_0$ is assumed to be constant and $\boldsymbol{J}_0$ is determined by the $q(r)$ profile, which is assumed to be of quadratic form and is given by $q(r=0)$ and $q(r=a)$. The first equation implies that we neglect the electrostatic mode. Equation (1) is used to replace z-components of $\boldsymbol{b}$, $\boldsymbol{v}$ and $\boldsymbol{E}$ and the ϕ-component of $\boldsymbol{j}$. Furthermore, equation (4) is inserted into (2) and additionally the curl operator is applied to (2) and (5). This leads to the following:

Maxwell's equations:

$$\mathrm{curl}\,\mathrm{curl}\,\boldsymbol{b} - \frac{\mathrm{i}\boldsymbol{b}}{\delta^2} = \frac{\mathrm{curl}(\boldsymbol{v} \times \boldsymbol{B}_0)}{\omega\delta^2} \tag{6}$$

Momentum equation:

$$\frac{-\mathrm{i}\omega\,\mathrm{curl}(\boldsymbol{v})}{V_\mathrm{A}^2} = \mu_0 \frac{\mathrm{curl}(\boldsymbol{j} \times \boldsymbol{B}_0)}{B_{z0}^2} + \mu_0 \frac{\mathrm{curl}(\boldsymbol{J}_0 \times \boldsymbol{b})}{B_{z0}^2} \tag{7}$$

Ohm's law:

$$\frac{1}{\sigma}\mathrm{curl}(\boldsymbol{j}) = \mathrm{curl}(\boldsymbol{v} \times \boldsymbol{B}_0) + \mathrm{i}\omega \boldsymbol{b} \tag{8}$$

It is assumed that the fields can be written in the variables, t, ϕ and z as Fourier components namely as $\boldsymbol{b}(r,\phi,z) = b(r)\exp(\mathrm{i}(m\phi - kz - \omega t))$ etc. Here, m is the azimuthal (poloidal) mode number, n the axial (toroidal) one, R_0 the major radius and q_res the resonance radius: $k = n/R_0 = m/q_\mathrm{res}$, i is the imaginary unit, V_A is the Alfvén speed, $V_\mathrm{A}^2 = B_{0z}^2/(\mu_0\rho)$, δ is the skin depth, $\delta^2 = 1/(\mu_0\sigma\omega)$ and σ is the electrical conductivity, which is assumed to be constant and is given as $\sigma_\parallel = 1127 \times 10^3 T_\mathrm{e}^{3/2}$ ($1/\Omega$m, T in eV).

Finally, the components of the vector equations can be cast in the following form (for the evaluation the MAPLE program was extremely useful). It should be remarked that the set of equations (6)–(8) results in nine equations for the six unknowns; the components b_z, v_z and j_φ were already eliminated by applying the div operator. We can verify that the third equation of each curl operator is identically fulfilled by the other two equations. Therefore, we write only the remaining relevant equations:

Maxwell's equations:

$$\frac{\mathrm{d}^2 b_r(r)}{\mathrm{d}r^2} + \frac{1}{r}\frac{\mathrm{d}b_r}{\mathrm{d}r} - \frac{(m^2+1)b_r(r)}{r^2} + \left(\frac{\mathrm{i}}{\delta^2} - k^2\right) b_r(r) - \frac{2\mathrm{i}m b_\varphi(r)}{r^2} + \frac{(mB_{0\varphi}(r)/r - kB_{0z})\mathrm{i}v_r(r)}{\omega\delta^2} = 0 \tag{9}$$

$$\frac{2\mathrm{i}m b_r(r)}{r^2} + \frac{\mathrm{d}^2 b_\varphi(r)}{\mathrm{d}r^2} + \frac{1}{r}\frac{\mathrm{d}b_\varphi(r)}{\mathrm{d}r} - \frac{(m^2+1)b_\varphi(r)}{r^2} + \left(\frac{\mathrm{i}}{\delta^2} - k^2\right) b_\varphi(r) + \frac{(B_{0\varphi}(r)/r - \mathrm{d}B_{0\varphi}(r)/\mathrm{d}r)\mathrm{i}v_r(r)}{\omega\delta^2} + \frac{(mB_{0\varphi}(r)/r - kB_{0z})v_\varphi(r)}{\omega\delta^2} = 0 \tag{10}$$

Momentum equation:

$$-\frac{\mathrm{i}\mu_0 J_{0z}(r) k b_r(r)}{B_{0z}^2} - \frac{\mathrm{i}\omega(\mathrm{d}v_r(r)/\mathrm{d}r + v_r(r)r)}{V_\mathrm{A}^2 kr} + \frac{\omega(m^2/kr^2 + k)v_\varphi}{V_\mathrm{A}^2} + \frac{\mathrm{i}\mu_0(kB_{0z} - mB_{0\varphi}(r)/r)j_r}{B_{0z}^2} = 0 \tag{11}$$

$$-\frac{\mu_0 J_{0z}(r)(\mathrm{d}b_r(r)/\mathrm{d}r)}{B_{0z}^2} - \frac{\mu_0(J_{0z}(r) + r(\mathrm{d}J_{0z}(r)/\mathrm{d}r))b_r(r)}{B_{0z}^2 r} - \frac{\mathrm{i}m\mu_0 J_{0z}(r) b_\varphi}{B_{z0}^2 r} - \frac{\omega m v_r(r)}{V_\mathrm{A}^2 r} - \frac{\mathrm{i}\omega(\mathrm{d}v_\varphi(r)/\mathrm{d}r + v_\varphi(r)/r)}{V_\mathrm{A}^2} + \frac{\mathrm{i}\mu_0(kB_{0z} - mB_{0\varphi}/r)j_z(r)}{B_{0z}^2} = 0 \tag{12}$$

Ohm's law:

$$-\frac{\mathrm{i}b_r(r)}{B_{0z}} + \frac{\mathrm{i}(kB_{0z} - mB_{0\varphi}(r)/r)v_r(r)}{\omega B_{0z}} - \frac{\delta^2\mu_0 rk(\mathrm{d}j_r(r)/\mathrm{d}r)}{mB_{0z}} - \frac{\delta^2\mu_0 k j_r(r)}{mB_{0z}} + \frac{\mathrm{i}\delta^2\mu_0(rk^2/m + m/r)j_z(r)}{B_{0z}} = 0 \tag{13}$$

$$-\frac{\mathrm{i}b_\varphi(r)}{B_{0z}} + \frac{(\mathrm{d}B_{0\varphi}(r)/\mathrm{d}r - B_{0\varphi}(r)/r)v_r(r)}{\omega B_{0z}} + \frac{\mathrm{i}(kB_{0z} - mB_{0\varphi}(r)/r)v_\varphi(r)}{\omega B_{0z}} - \frac{\mathrm{i}\delta^2 k\mu_0 j_r(r)}{B_{0z}} - \frac{\delta^2\mu_0(\mathrm{d}j_z(r)/\mathrm{d}r)}{B_{0z}} = 0 \tag{14}$$

These are six complex differential equations, yielding 12 real ones. The electric field has been eliminated from the differential equations. Using the solution of the vector $j(r)$, the electric field vector is derived using equation (3). This gives in total 18 coupled differential equations of partially first and partially second-order.

The plasma area is only part of the problem. Let us denote the plasma area as area I as shown in figure 2. This part is surrounded at first by a vacuum, area II, then the coil structure, area III, which has a width Δ and a triangular current distribution—zero at both boundaries and maximum in the middle—and finally an outer vacuum region again, area IV.

For technical reasons we take in this domain infinity at a radius of 10 m.

In order to obtain solutions of the system, boundary conditions have to be specified. All quantities are assumed to be continuous at the transition of the different areas. This means, in particular for the electric field, that we neglect electrostatic solutions, which have a charge formation at the boundary between area I and area II. The external current is specified by the maxium amplitude in area III. All vector quantities are assumed to vanish both at the axis and at infinity, and on the axis. The radial and azimuthal vector components are naturally zero at the axis and $j_z(r = 0)$ is assumed to grow on-axis as a Bessel function of order m and vanishes, therefore.

4. The computer code

The equations [9–14] were solved using PDE2D, a commercially-available finite element code (www.pde2d.com). This code solves general systems of nonlinear, time-dependent, steady-state and eigenvalue problems in general two-dimensional geometry and a wide range of simple three-dimensional geometry. For one-dimensional problems such as ours, a collocation finite element method is used, with cubic Hermite basis functions. This means, each unknown is expanded as a linear combination of the basis functions $H_k(x)$ and $S_k(x)$, where H_k and S_k are piecewise cubic polynomials which are continuous and have continuous first derivatives. The unknown coefficients in these expansions are determined by imposing the boundary conditions at the end points, and requiring that the differential equations be satisfied exactly at two collocation points in each subinterval $[x_j, x_{j+1}]$. A system of complex equations such as ours must be broken into its real and imaginary parts, but this is easily accomplished using the complex arithmetic capabilities of FORTRAN.

The grid of the calculation must be particularly dense near the resonance radius and near the antenna. In total, 1401 grid points are taken using

20% for $0 \leqslant r \leqslant 0.97 r_{\rm res}$
20% for $0.97 \leqslant r \leqslant 1.03 r_{\rm res}$
10% for $1.03 r_{\rm res} \leqslant r \leqslant a$
10% for $a \leqslant r \leqslant r_{\rm antenna}$
10% for $r_{\rm antenna} \leqslant r \leqslant r_{\rm antenna} + \Delta$
10% for $r_{\rm antenna} + \Delta \leqslant r \leqslant 2 r_{\rm antenna}$
20% for $2 r_{\rm antenna} \leqslant r \leqslant r_{\rm infinity}$

Typical values of the boundary constants are: $r_{\rm res} \cong 0.426$ m, $a = 0.47$ m, $r_{\rm antenna} = 0.5325$ m, $\Delta = 0.01$ m and $r_{\rm infinity} = 10$ m.

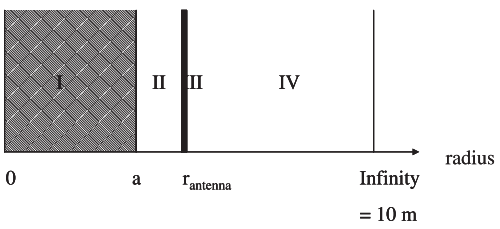

Figure 2. The four areas for the solution of the MHD model: area I represents the plasma which is governed by MHD equations, areas II and IV are vacuum and area III represents the external current layer. 'Infinity' is taken at a radius of 10 m.

5. Results

5.1. Boundary plasma of $T = 50\,eV$

For the calculations, the following 'magnetic' data were used: $B_{0z} = 2$ T, $R_0 = 1.75$ m, $q(r = 0) = 0.7$, $q(r = r_{\rm res}) = 3$, $q(r = a) = 3.5$ (parabolic q-profile). The reference plasma is: density at the edge (assumed to be constant in the edge) $n_{\rm e} = 1.0 \times 10^{19}\,{\rm m}^{-3}$; electron temperature, $T_{\rm e} = 50$ eV (assumed to be constant in the edge). The DED has the values: DED-current = 15 kA, $m = 12$, $n = 4$, which results in the value of the axial wave vector $k = 2.286\,{\rm m}^{-1}$. The DED frequency f is the main parameter in this study; the frequency value assumed is the difference in frequency between the plasma rotation and the DED field.

For these data, the Alfvén velocity amounts to $V_{\rm A} = 9.755{\rm E}{+}06\,{\rm m\,s}^{-1}$, the conductivity to $\sigma = 0.3985{\rm E}{+}06$ $[1/(\Omega{\rm m})]$ and the skin depth to $\delta = 0.01783$ m for a frequency $f = 1$ kHz.

Figure 3 shows the radial distribution of the real and imaginary parts of the b_φ field. As expected, the real part of b_φ 'jumps' at the location of the antenna from a negative value inside the antenna to a positive one outside. Due to the high multipolarity of the DED coil system, the field decays strongly in both directions away from the antenna. For the vacuum solution, one expects a decay of roughly $b_\varphi(r)/b_\varphi(r = r_{\rm antenna}) \approx (r/r_{\rm antenna})^{\pm m}$ (plus sign inside, minus sign outside the antenna). At the location of the resonant radius, the effect of the induced shielding current is rather small for the B-field at the given frequency of 1 kHz. The real part of b_φ decreases, the imaginary part exhibits a similar structure as the real part at the antenna radius. This indicates the presence of currents excited near the resonant surface; the current obviously has a phase shift with respect to the external one.

The imaginary part of the radial magnetic field is its dominant component as shown in figure 4 and as expected

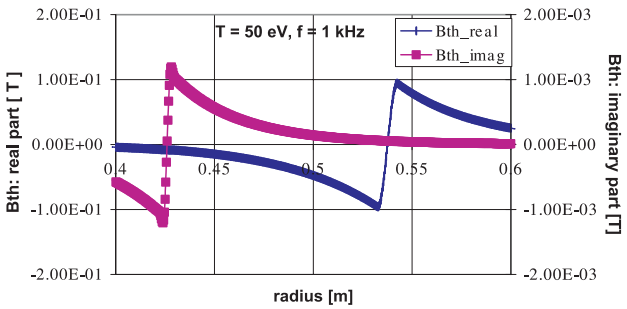

Figure 3. Real and imaginary part of the azimuthal component of the magnetic field for $f = 1$ kHz.

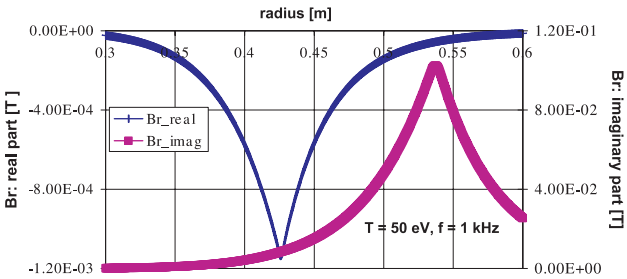

Figure 4. Radial component of the magnetic field for $f = 1$ kHz.

from the 90° phase shift between b_r and b_φ; the imaginary part is maximum at the antenna from where it decays in both directions. This is expected because b_r is continuous at a current sheath while the azimuthal component should obey a jump condition. At the resonant surface, the real part of b_r is an important one and shows a shape similar to the imaginary part of b_φ at the antenna.

The electrical current in the axial direction is about two orders of magnitude larger than the azimuthal one and another two orders of magnitude larger than the radial one. Figure 5 shows the axial current density as a function of the radius, however, at a much higher radial resolution. The current distribution is symmetric with respect to the resonant radius, and the real and imaginary parts are of about the same size. The full width of the current layer amounts to about 5 mm only for the given frequency and is about a factor of 3 smaller than the skin width. The detailed shape of the real and imaginary part of the j_z current distribution depends on the temperature and frequency and it reflects the phase shift of the current.

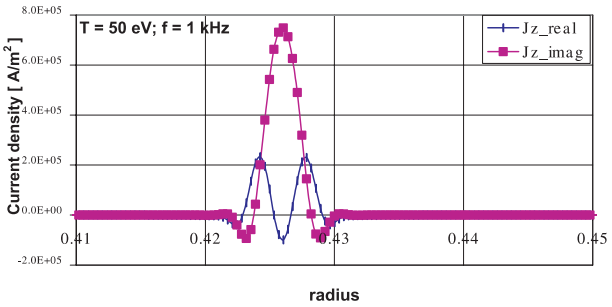

Figure 5. Radial distribution of the axial current. One finds a strong enhancement at the resonance layer.

Of particular interest is the relation between the magnetic islands and the current layer. The magnetic island is obtained by projecting the magnetic field lines into the plane perpendicular to the resonant magnetic field lines at $q = 3$. The result of such a projection is shown in figure 6 in the plane spanned by the radial coordinate and the bi-normal. One sees a large and strongly asymmetric magnetic island. Since we have chosen the same radial width of the figure as in most other figures, the outward part of the island is not yet shown. A closer analysis shows that the field lines of the islands go even beyond the external perturbation coils. They actually have the shape that we discussed in a previous paper [20]. It is essentially the island generated from the superposition of the equilibrium field and the external perturbation. It is obvious that this field has a strong influence also at the resonance. However, the island does not extend much beyond the resonance layer.

The 'normal' islands in picture MHD describe a different property than that shown here; its shape should not be determined by the electrical current in the external coils but by the current flowing in the island itself. In order to visualize this second type of island we start with the magnetic field data used in figure 6 but we subtract the field perturbation obtained for the case of a DED frequency of 10 Hz, which is essentially the vacuum field. Otherwise the same projection is performed. The result of this operation is shown in figure 7. One sees that the island obtained in this way is clearly restricted to the radius close to the resonant surface.

For comparison of the island shape and location, we plot the current density profile as a contour plot in figure 8. One sees that the island formed by the internal current is phase shifted by 90° with respect to the complete island. In our interpretation the current in this island is induced according

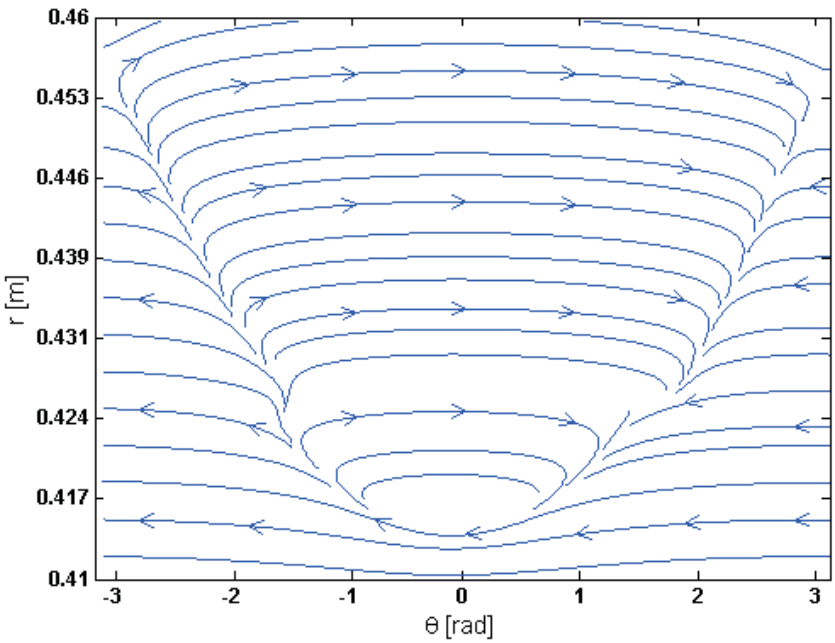

Figure 6. Magnetic island generated by the superposition of the equilibrium field and the perturbation field. The structure is generated by the projection $(B_0 + B_1)k$ into the plane perpendicular to the magnetic field of the resonance zone. The island grows towards the DED coils and gives it a strongly asymmetric shape with respect to the resonance layer. The field lines go even beyond the DED coils. The conditions are the same as in figure 4.

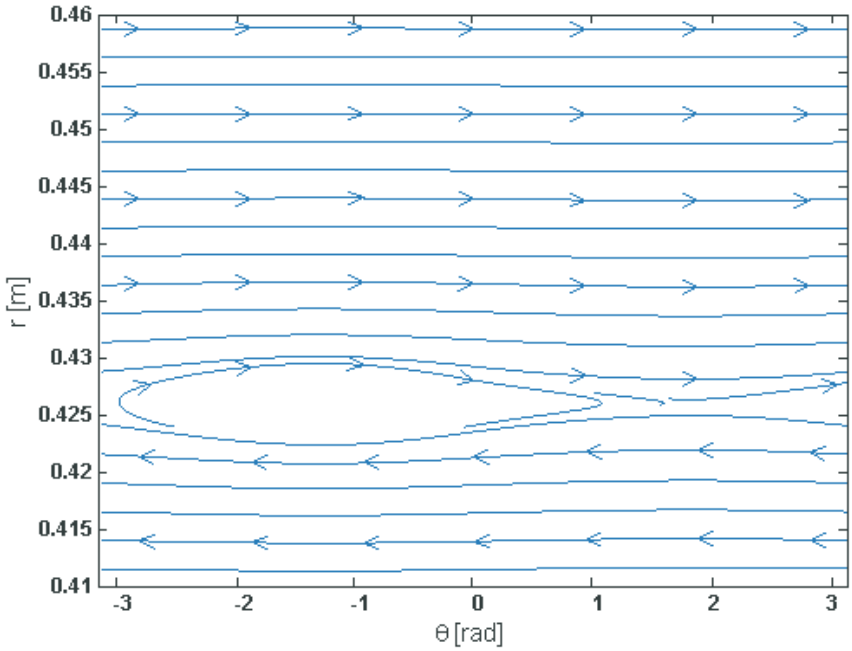

Figure 7. The 'MHD-island' is the part of the island generated by the electrical current (figure 5) flowing at the resonance layer. It is derived in the same way as figure 6, however additionally subtracting the vacuum solution. This island is shifted by 90° with respect to the original island of figure 6.

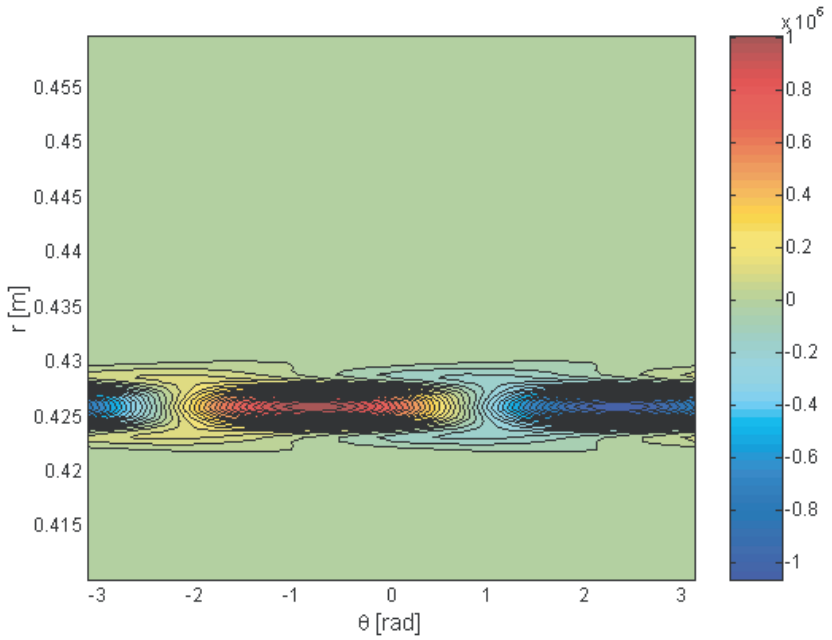

Figure 8. Contour lines of the current density which form the 'MHD-island'. The current is the same one as plotted in figure 5.

to $\mathrm{d}B/\mathrm{d}t$ and is slightly unsymmetrical; near the resonance layer it looks slightly shifted to the left. The superposition of a symmetric vacuum island and the one induced by the excited current would lead to the observed deformation. The width of the channel of the electrical current has about the same size as the island corresponding to this island. The positive current maximum is located at the O-point of the island and the negative minimum at the X-point.

Figure 9 shows the resulting phase distribution. The phase shift is rather symmetric with respect to the resonance layer. This may be remarkable in so far as for a 'normal' skin type shielding current one would expect a monotonic increase of the phase from the outside to the inside.

The currents flowing at the resonance layer generate a force on the plasma and consequently a plasma flow. The strongest component of the plasma flow is in the azimuthal direction and it is more than an order of magnitude larger than the other components. Figure 10 shows the distribution of the azimuthal (top part) and radial (bottom part) components of the plasma velocities. The azimuthal velocity distribution is

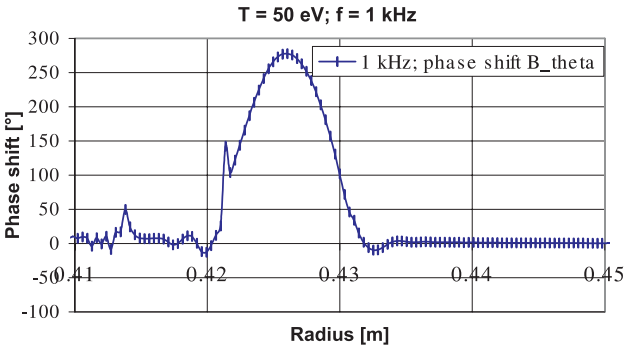

Figure 9. Radial distribution of the phase shift of the electrical current. The phase drops symmetrically away from the resonance layer.

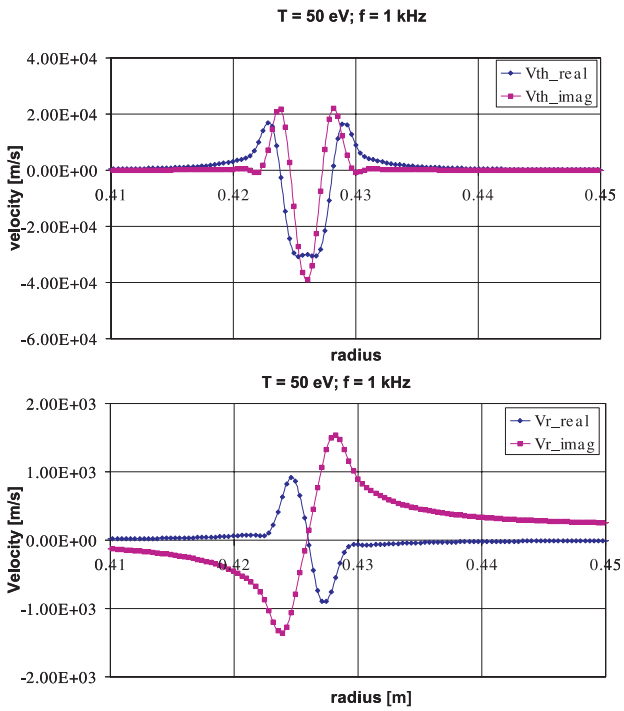

Figure 10. Azimuthal and radial components of the velocity pattern. The detailed analysis of the real and imaginary parts show a double vortex structure around the resonance layer.

symmetric and the radial one anti-symmetric with respect to the resonance layer; in particular, the radial velocity is zero. A more detailed analysis shows that the plasma flow forms a double vortex pattern, one vortex on each side of the resonance. The width of the resonance corresponds to that of the electrical current.

When the frequency increases, the shielding effect becomes larger and the interaction width becomes wider for the azimuthal magnetic field (top figure) and for the velocity distribution (bottom figure), as one can see in figure 11. The amplitude of the velocity does not grow substantially when the frequency increases from 1 to 10 kHz; the width increases from 0.5 cm to about 1 cm. Increasing the frequency is equivalent to decreasing the skin width δ from 1.7 to 0.56 cm. Thus, the width of the current layer is now smaller than the skin depth.

Towards low frequencies, both the amplitude and the width of the perturbation decrease. At a frequency of 100 Hz,

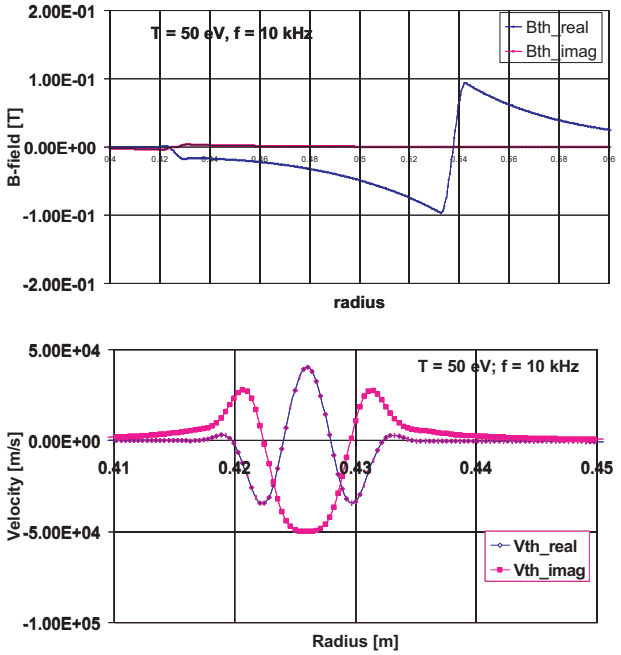

Figure 11. Magnetic field and velocity distribution at 10 kHz.

the amplitude of the velocity drops by a factor of about 4–1 $\times$ 10^4 m s^{-1} and the width is reduced to about 2 mm. It is obvious that at low frequencies the model breaks down because the viscosity of the plasma is neglected. This viscosity should smear out the strong gradients in the flow velocity. It will be an important experimental task to search for the predicted flow pattern in the whole frequency domain and to investigate whether they exist or destroyed, e.g. by viscosity or by a Kelvin–Helmholtz instability which occurs in a strongly sheared flow.

5.2. *Core plasma of $T = 500\,eV$*

The DED can be operated in different modes. The mode described up to now corresponds to the $m/n = 12/4$ mode, which predominantly influences the plasma edge. In order to study the influence on islands deep inside the plasma one would choose, e.g. the coarser $m/n = 3/1$ base mode. The DED perturbation spectrum has several islands such that not only the $q = 3$ surface is influenced but even the $q = 2$ and $q = 1$ surfaces. Here, the temperature is of course much higher than the 50 eV assumed up to now. We have, therefore, also made runs with a typical temperature of 500 eV, but for the $m/n = 12/4$ mode scenario in order not to vary too many parameters. The temperature of the plasma enters into the problem via the electrical conductivity and influences the skin width δ. A variation of the temperature is, therefore, equivalent to a variation of the frequency. This is indeed the result of these runs; the layer of the perturbation current and the velocity flow field are indeed considerably wider than at the lower temperature. This finding should ease the observation of the plasma flow pattern of the central islands, e.g. by charge exchange recombination spectroscopy (CXRS).

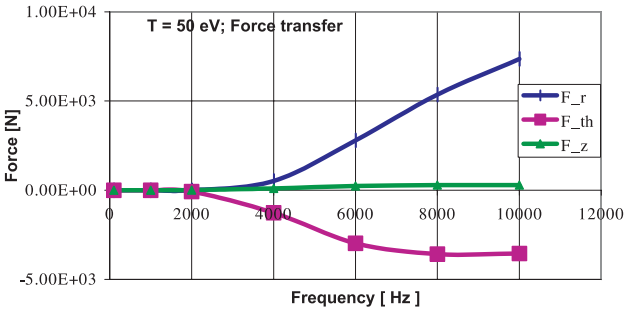

Figure 12. Force transfer function at 50 eV, which is representative of the edge region of the plasma.

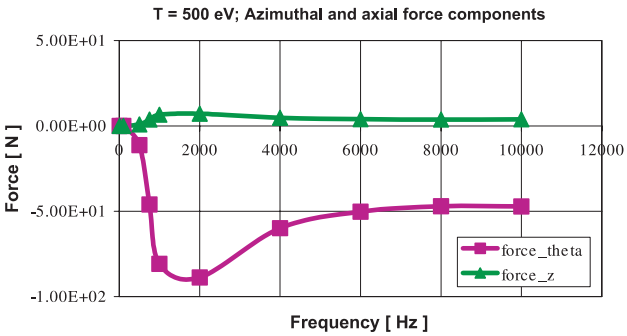

Figure 13. Force transfer function at $T_e = 500$ eV. The higher value of T_e represents a more central interaction zone (even though the interaction radius is not changed). The different trends in figures 12 and 13 may require a different optimization for edge and core with respect to force transfer.

5.3. Force transfer

The integration of the term $\int \langle (j + j^*) \times (b + b^*) \rangle 2\pi r \, \mathrm{d}r$ yields the force transferred from the wave field to the plasma; the brackets $\langle\,\rangle$ indicate the time average and j and b stand for the perturbation quantities and their complex conjugates j^* and b^*, respectively. Figure 12 shows the force transfer function for a 50 eV boundary plasma depending on the perturbation frequency; however, for the application on the TEXTOR DED the value should be divided by a factor of three because the coils cover roughly $\frac{1}{3}$ of the circumference only. For this condition, the force transfer at a frequency below a few kilohertz is rather small. The force transfer function in the radial direction is monotonically increasing and is the dominant quantity at high frequencies. Nevertheless, we neglect this force component because in the radial direction the pressure and equilibrium terms dominate anyway. This is different in the azimuthal and axial directions where no equilibrium accelerating force exists (at least not within this model). It is remarkable that the force transfer in the azimuthal direction exhibits a maximum at a frequency in the range $f = 8$–10 kHz. However, this maximum is expected from the analysis of the inductive motor (and it has also been described in a previous publication [17]; the frequency and the amplitude of the maximum torque transfer of the older and simpler model agree rather well with the present values. The force in the axial (toroidal) direction is an order of magnitude smaller than in the poloidal direction as one expects from the inclination of the DED coils. Nevertheless, this component of force is not inhibited by neoclassical effects and can possibly accelerate the plasma. The maximum value of this force is about the same as the force from the tangential neutral beam injection (NBI); because NBI leads to a substantial plasma rotation, it can be expected that the DED also would accelerate a plasma or conversely—in the static mode of DED operation—it would reduce the rotation of a previously spinning plasma. These investigations are currently an important topic of research for the fusion community, in particular in the stabilization of wall resistive modes [21, 22].

In figure 13 the force transfer function of the azimuthal and axial force components is shown assuming a plasma temperature of 500 eV but for otherwise the same configuration as in figure 12. The maximum of the force transfer function has now moved to a smaller frequency, namely to about 2 kHz. This shift is expected from the change of the skin width as discussed above. Nevertheless, it has important consequences for the optimization of the interaction between the plasma and the external DED current. In order to have a strong force transfer at the plasma edge, one would like to operate at a large frequency difference between the plasma and the wave field while for the plasma core a much lower frequency difference may be more favourable. In order to allow for the full flexibility, the DED has been laid out to operate at seven frequencies in the range between 1 and 10 kHz, and this should provide sufficient insight into the underlying physics.

6. Summary and outlook

A one-fluid MHD model in cylindrical geometry for the penetration of a perturbation field into a plasma has been analysed. The resulting set of 18 coupled ordinary differential equations of up to second-order are computed by a commercial numerical finite element solver, PDE2D. The analysis shows that—as expected—the external magnetic field penetrates nearly unperturbed into the plasma edge; at the resonance layer, where the external coils are parallel to the internal magnetic field lines, a strong shielding current is generated. Depending on the frequency difference between the external field and the plasma, the width and the amplitude of the shielding current vary; towards high frequency, the amplitude and width grow while towards low frequency both quantities decrease. The model predicts that the shielding current is connected with a localized flow of the plasma. The width of the flow pattern has a similar value as the one of the current layer. The analysis shows that the flow corresponds to a double vortex structure at both sides of the resonant surface. At very low frequencies, e.g. below 100 Hz, the width of the current and flow structures become of the order of a millimetre or lower; it is expected then that viscosity effects become important and damp the strong gradients of the plasma flow.

The TEXTOR DED is flexible enough to excite both the resonances at the plasma edge—which may be the standard case—and in the core. For analysing the interaction effect of the perturbation with the plasma in the core, we have increased the plasma temperature by one order of magnitude. Two important parameters enter the MHD model, the skin depth and the Alfvén velocity. When keeping the plasma density constant (Alfvén velocity), the variation of the plasma temperature in the skin width corresponds to a variation of the frequency.

Consistently, at higher plasma temperatures a wider interaction width of the induced current and flow pattern is observed.

The force transfer function as a function of frequency always has a maximum. For the edge conditions, the maximum is at the high frequency end of the operation range of the DED while for the core one expects this maximum at the lower frequency end. Therefore, specific optimizations for edge and core interactions will be required.

We consider the model presented above as a good working approximation in order to compare experimental results, which are soon coming up with a simple model. Our expectation is that the model has already enough basic features for such a comparison. We are, of course, aware of the shortcomings of the model and it will be a task of the experiments to show which effect plays an additional important role. Here, we list some of those effects:

(a) The model neglects the nonlinearities. Nonlinearities enter in two ways. The first nonlinearity enters in the conventional way namely due to the nonlinear terms of the equation. It has been estimated by Pankratov *et al* [23], that the nonlinear terms become important for a DED current higher than 5 kA. It is expected that the nonlinearities lead to a growth of modes as, e.g. modelled by Lazzaro *et al* [24] or Fitzpatrick [3, 22]. These modes may lead to a locking of the plasma flow to the modes.

(b) The second nonlinearity results from the ergodization of the background magnetic field. The DED generates perturbations with different helicities; the overlap of these perturbations generates the ergodization. Since the induced electrical current near the resonance layer flows parallel to the magnetic field lines, it is expected that a bending and deformation of the magnetic field lines would also widen the layer of the electrical current. Unfortunately, there is no theory yet which treats, e.g. tearing type modes with an ergodized background magnetic field structure. We expect that the effects of ergodization will play a role for perturbation currents larger than 2–5 kA. The ergodicity may reduce the edge temperature; the modified temperature profile may influence the edge electric field, which then modifies the plasma rotation.

(c) Our model is a single fluid MHD one. Therefore, effects of the electric field inside the plasma are neglected. At the plasma boundary, the electric field generates ion and electron drift modes, which are often observed in tokamak discharges. The interaction of the external perturbation field with these modes may be an important effect, in particular, because the frequency of the internal and external modes have a similar value.

(d) The model is cold MHD and neglects acoustic waves. Acoustic waves have a very short wavelength and their integration requires sophisticated methods [25]. It may be that the acoustic waves play a role at the resonance.

(e) It has already been mentioned that our model contains a dissipative effect only in the form of the resistivity. In particular, at a small width of the resonance layer other effects such as viscosity are expected to play an important role as well.

(f) An important topic for future considerations is also the stability and growth of the induced island pattern. It is expected that the stability depends on the distribution of the equilibrium current. In addition, the nonlinear regime is of interest where additional electrical currents may be excited in the 'seed island' provided by the DED.

(g) In the given model all effects of toroidicity have been neglected. It is obvious that this part needs additional attention.

References

[1] Special issue: Dynamic Ergodic Divertor 1997 *Fusion Eng. Des.* **37** 335–450
[2] Abdullaev S.S., Eich Th. and Finken K.H. 2001 *Phys. Plasmas* **8** 2739
[3] Fitzpatrick R. and Hender T.C. 1991 *Phys. Rev.* B **3** 644
[4] Jensen T.H., Leonard A.W., LaHaye R.J. and Chu M.S. 1991 *Phys. Fluids* B **3** 1650
[5] Jensen T.H., Leonard A.W. and Hyatt A.W. 1993 *Phys. Fluids* B **5** 1239
[6] Hurricane O.A., Jensen T.H. and Hassam A.B. 1995 *Phys. Plasmas* **2** 1076
[7] Kikuchi Y., Uesugi Y., Takamura S. and Elfimov A.G. 2003 *Europhys. Conf. Abst.* A **24** P-2.119
[8] Jensen T.H. and Leonard A.W. 1991 *Phys. Fluids* B **3** 3422
[9] Bigliari H., Diamond P.H. and Terry P.W. 1990 *Phys. Fluids* B **2** 1
[10] Hender T.C. *et al* 1992 *Nucl. Fusion* **32** 2091
[11] LaHaye R.J. *et al* 1992 *Phys. Fluids* B **4** 2098
[12] Scoville J.T. *et al* 1991 *Nucl. Fusion* **31** 875
[13] Kobayashi M. *et al* 2000 *Nucl. Fusion* **40** 181
[14] Foster M.S., McCool S.C. and Wooton A.J. 1995 *Nucl. Fusion* **35** 329
[15] Faulconer D.W. and Koch R. 1997 *Fusion Eng. Des.* **37** 399
[16] Elfimov A.G., Petrzilka V. and Tataronis J.A. 1994 *Phys. Plasmas* **1** 2882
[17] Finken K.H. 1999 *Nucl. Fusion* 39 707
[18] Finken K.H. *et al* 2001 *Nucl. Fusion* **41** 503
[19] Pankratov I.M., Omelchenko A.Ya. and Olshansky V.V. 2002 Problems of atomic science and technology *Series: Plasma Phys.* **8**
[20] Finken K.H. 1997 *Nucl. Fusion* **37** 583
[21] Fitzpatrick R. 1993 *Nucl. Fusion* **33** 1049
[22] Fitzpatrick R. and Yu E.P. 1998 *Phys. Plasmas* **5** 2340
[23] Pankratov I.M., Omelchenko A.Ya. and Olshansky V.V. 2003 private communication (Juelich)
[24] Lazzaro E. *et al* 2002 *Phys. Plasmas* **9** 3906
[25] Faulconer D.L. and Juelich 2003 private communication